binds with either a sulfoxide or thioether donor and whether five-coordinate intermediate II or III reacts with ligand **3**.

Inspection of Figure 5 and the scheme in the supplementary material reveals that five-coordinate intermediate II with the *trans*-dihalo configuration cannot give the observed products but would give only the desired all-trans complex. Since this isomer is never observed, this pathway would not be operative. This means that the initial trigonal-bipyramidal intermediate, *trans*-$RuBr_2(S(CH_2)_4)_3$, would undergo an isomerization (pseudorotation) to yield a *cis*-dibromo five-coordinate intermediate (structure III of Figure 5) and finally complexation with ligand **3** would yield the observed products. An analysis of all the possible pathways available for coordination of ligand **3** to five-coordinate intermediate III of Figure 5 is presented in the supplementary material. Nevertheless, observed geometric isomers C (**10**) and E(**9**) are indeed predicted from the complexation pathways that utilize five-coordinate intermediate III (Figure 5).

Thus, it appears that the use of a linear tridentate ligand to generate the all-trans 2,2,2 complex will not succeed. This apparently arises because the *trans*-dihalo geometry of the five-coordinate intermediate is in a very unfavorable equilibrium with the five-coordinate intermediate with the *cis*-dihalo geometry (III of Figure 5). Consequently, the *cis*-dihalo geometry will be more favorable in the products of the substitution reactions, thus limiting their usefulness for the synthesis of the all-trans complexes. In the catalytic situation in which monodentate ligands are present, this problem can apparently be overcome. The subtle electronic factors favoring the cis geometries can be overridden by steric factors that favor the all-trans geometry. When bulkier monodentate substrates are used, the faster rates that are observed[3] are consistent with the formation of a higher concentration of the desired all-trans complex, although very bulky thioether ligands (t-Bu_2S) afford no catalytic activity since complexes of the stoichiometry $RuX_2(R_2S)_2(R_2SO)_2$ do not form in this case.

Acknowledgment is made to L. C. Strickland (of these laboratories) for his assistance with the crystal structure investigation, to R. E. Shumate for his assistance with the syntheses, and to Professor Devon Meek of The Ohio State University for useful discussions.

Registry No. **2**, 101653-80-9; **3**, 101835-53-4; **5**, 101810-60-0; **6**, 101835-55-6; **7**, 101835-54-5; **8**, 101835-56-7; **9**, 101835-57-8; **10**, 101915-10-0.

Supplementary Material Available: Tables of H atom parameters, anisotropic thermal parameters, bond lengths and bond angles, and the numerical description of the pseudomirror plane and a figure illustrating the possible substitution pathways for the reaction between *trans*-$RuBr_2(\overline{S(CH_2)_3CH_2})_4$ and ligand **3** (5 pages). Ordering information is given on any current masthead page. According to policy instituted Jan 1, 1986, the tables of calculated and observed structure factors (17 pages) are being retained in the editorial office for a period of 1 year following the appearance of this work in print. Inquiries for copies of these materials should be directed to the Editor.

Contribution from the Laboratoire de Dynamique des Cristaux Moléculaires, ERA No. 465 du CNRS, Université des Sciences et Techniques de Lille, 59655 Villeneuve d'Ascq Cédex, France, and ER No. 139 du CNRS, Laboratoire de Chimie Quantique, Université Louis Pasteur, 67000 Strasbourg, France

Dynamic, Static, and Theoretical Electron Deformation Density for Binuclear Transition-Metal Complexes: Dicobalt Hexacarbonyl Acetylene

F. Baert,[1a] A. Guelzim,[1a] J. M. Poblet,[1b] R. Wiest,[1c] J. Demuynck,[1c] and M. Bénard*[1c]

Received July 31, 1985

The electron deformation density distribution in $Co_2(CO)_6R_2C_2$ ($R = C(CH_3)_3$) has been obtained from low-temperature X-ray and neutron data and from theoretical wave functions at the Hartree–Fock and configuration interaction levels. The experimental determination of the deformation density of (t-Bu_2C_2)$Co_2(CO)_6$ at 122 K (space group $P\bar{1}$, a = 8.289 (2) Å, b = 8.400 (2) Å, c = 13.552 (2) Å, α = 88.67 (2)°, β = 94.45 (2)°, γ = 106.75 (4)°, Z = 2) does not show accumulation of density along the Co–Co line (Co–Co = 2.462 Å). The static deformation density maps obtained from multipolar refinement display two electron depopulation regions around each Co atom, separated by two peaks. An axis of minimum deformation density can be defined in the vicinity of each cobalt. This axis is collinear with the direction of the bent metal–metal bond defined by quantum-chemical LCAO calculations. The theoretical maps at SCF and CI levels display similar depopulation regions, but four distinct peaks are found around each metal. A "bent-bond peak" is obtained between the acetylene carbon atoms in both the experimental and the theoretical maps. The position of the peak, which is shifted away from the metal–metal line, results from the displacement of the π overlap, in turn caused by the distortion of the acetylenic system. These experimental and theoretical results are compared with the density maps previously published for the isolobal complex $Ni_2(C_5H_5)_2C_2H_2$. Much similarity is obtained between the distributions computed for both complexes and with the experimental maps of the dicobalt system. It seems that the disagreement with the experimental maps of $Ni_2(C_5H_5)_2C_2H_2$ is a consequence of the crystalline acentric and disordered structure of the dinickel complex. Fragment deformation densities have been computed for $Co_2(CO)_6C_2H_2$. The corresponding maps display an important accumulation of density in the π^* orbital of the acetylene carbons, directed toward the Co atoms. The Mulliken population analysis shows that back-donation corresponds to a charge transfer of 0.88 e, balanced by a σ-donation transfer of the same magnitude. A significant peak is also obtained at the center of the metal–metal bent bond. The results illuminate the synergic bonding characteristic of these complexes, where metal–metal interaction, the σ donation, and the π back-donation are involved.

Introduction

The relatively small deformation of the valence part of the electron cloud is known to be the key for bonding energy and molecular structure. The more or less accurate analysis of the electron density distribution in molecules has been for a long time the privilege of theoretical chemistry, which can obtain such a distribution from a computed wave function. Over the last 15 years, however, increasingly accurate X-ray or neutron diffraction experiments have allowed us, according to the term coined by Coppens, to "see the electrons".[2]

Another condition for ensuring the chemical interest of these experimental density distributions is to focus the discussion of the results on this part of the electron cloud, which has been reorganized by chemical bonding. This is obtained by substracting from the observed density distribution of the system another distribution

(1) (a) Laboratoire de Dynamique des Cristaux Moléculaires. (b) ER No. 139 du CNRS. Permanent address: Department de Quimica Fisica, Facultat de Quimica, Pz. Imperial Tarraco 1, Tarragona 43005, Spain. (c) ER No. 139 du CNRS.

(2) Coppens, P. *J. Chem. Educ.* **1984**, *61*, 761.

0020-1669/86/1325-1830$01.50/0

computed for the "promolecule", a fictitious system in which all atoms considered at their correct geometrical position are supposed isolated, neutral, and spherically averaged and are supposed in their ground state. The resulting "deformation density" distribution pictures the displacement of the electron cloud generated by chemical bonding.

Despite the lack of any chemical interaction assumed in the definition of the promolecule, this collection of spherical atoms is nevertheless closely related to the studied system since both the real and the fictitious molecules correspond to the same set of atoms similarly located in space. Using the promolecule as a reference for picturing the electron reorganization in a given system can therefore make the picture somewhat dependent upon the model molecule. This can be a drawback to a clear chemical interpretation of the deformation density maps. Recent examples of rather puzzling features obtained in deformation density maps have questioned the use of the promolecule as a reference.[3,4]

Similar problems of interpretation have been raised by recent X-ray diffraction experiments carried out on binuclear transition-metal complexes.[5] Joint experimental and theoretical studies have contributed however to clarify the situation for this type of molecule.[6] For instance, the lack of any significant observed electron buildup in most single and multiple bonds between metals of the first transition row has been related to the contracted character of the metal 3d orbitals and to the subsequently small d–d overlap in the usual range of metal–metal bond lengths.[7]

For a particular binuclear system $Ni_2(C_5H_5)_2C_2H_2$, however, an important disagreement was obtained between the observed and the computed deformation density distributions in the region of the metal–metal bond.[9,10] These conflicting results have prevented chemical analysis of the density maps for this complex. We therefore decided to investigate the observed and computed deformation density distributions for $Co_2(CO)_6C_2R_2$,[11] a binuclear complex that is isolobal with the dinickel system. A special effort was made in the present study to eliminate or to investigate the possible causes of discrepancy between the observed and the computed results for the earlier case, namely the following:

(i) An acentric or disordered crystal structure may occur. Contrary to the case of $Ni_2(C_5H_5)_2C_2H_2$,[9] the crystals of $Co_2(CO)_6C_2R_2$ are centrosymmetric for R = *t*-Bu, CF_3, and CH_2OH (but not for R = COOH). No disorder was discovered during the refinement. This makes simpler and less ambiguous the calculation of difference densities from observed data.[12]

(ii) The effect of thermal motion is a cause of discrepancy. Static deformation maps were obtained from a multipolar refinement of the observed data. These maps can in principle be compared directly with the results of ab initio MO calculations carried out on an isolated and motionless ideal molecule.

(iii) The truncation of the Gaussian basis set may influence the computed density distribution. A relatively extended basis set (triple ζ for 3d, double ζ for 4s) was therefore used to describe the metal atoms.

Table I. Least-Squares Refinements[a]

	full data	high order >0.75 Å^{-1}	high order >0.85 Å^{-1}	model
no. of reflcns above $n[\sigma(I)]$	3	2	2	3
N_o	9869	4507	2811	9869
N_v	218	217	217	349
G	1.47	1.21	1.20	1.21
$R(F)$	0.024	0.033	0.042	0.021
$R_w(F)$	0.036	0.039	0.043	0.030
$R(F^2)$	0.036	0.052	0.064	0.031
$R_w(F^2)$	0.067	0.072	0.081	0.055

[a] $G = [\sum w\Delta^2/(N_o - N_v)]^{1/2}$; $R(F) = \sum(|F_o| - |F_c|)/\sum|F_o|$, $R_w(F) = [\sum w(|F_o| - |F_c|)^2/\sum wF_o^2]^{1/2}$, and corresponding expressions for F^2; N_o = number of observations; N_v = number of variables.

(iv) The electron correlation may affect computed density maps. A medium-size configuration interaction (CI) expansion (10 400 configurations) was carried out, involving all single and double excitations from a basis of 34 MO's characterized by important populations of metal 3d electrons.

Experimental Section

The structure of $(t\text{-}Bu_2C_2)Co_2(CO)_6$ was determined first by Cotton, Jamerson, and Stults;[13] then a neutron study was undertaken by Gregson and Howard.[15] A preliminary X-ray diffraction analysis was also carried out by Baert, Gregson, and Howard. No deformation density distribution has been reported up to now for this complex.

Baert, Guelzim, and Coppens[11] have reported X-ray crystal structures of three related compounds where R = COOH, CH_2OH, CF_3. The metal–metal distance evolves between 2.460 (2) and 2.476 (2) Å and seems independent of the electronegativity of the substituents.

Synthesis. All operations were carried out in an atmosphere of dry nitrogen. Solvents were dried over potassium benzophenone and were distilled under nitrogen just prior to use.

The synthesis of $(t\text{-}Bu_2C_2)Co_2(CO)_6$ was first reported by Cotton et al.[13] This compound was prepared by allowing an equimolar mixture of $Co_2(CO)_8$ and $t\text{-}Bu_2C_2$ in hexane to react at ambient temperature for 24 h. The reaction solution was filtered and the filtrate evaporated to dryness in vacuo at ambient temperature. The crude product was recrystallized from pentane at −40 °C to yield large deep maroon crystals.

Data Collection. The single-crystal X-ray data were collected on an automated Philips PW 1100 four-circle diffractometer at 122 (0.5) K using monochromated Mo K$\bar{\alpha}$ radiation (λ = 0.7107 Å) and the self-regulating cold-gas-flow cooling device manufactured by Leybold-Heraeus. Twenty-five high-angle reflections with well-resolved Kα_1 peaks were centered and used to calculate the cell dimensions.

The data set was collected on one crystal of approximate dimensions 0.31 × 0.11 × 0.13 mm and a volume of 5.240 × 10^{-3} mm^3. Data were collected in a θ–2θ step scan mode up to 2θ = 100°. Only equatorial reflections were measured twice. The full-reflection profiles were analyzed as described previously.[14] Lorentz polarization factors were applied, and an absorption correction was made (μ = 19.56 cm^{-1}) by using the gaussian integration method. The transmission factor varied between 0.87 and 0.90.

Least-Squares Refinements. Positional and thermal parameters from the neutron study of Gregson et al.[15a] at the same temperature were used as a starting set in a least-squares minimization of $\sum w(F_o^2 - k^2F_c^2)^2$ where $1/w = \sigma^2 = \sigma_{counting}^2 + (0.02F_o^2)^2$. Scattering factors and anomalous dispersions were taken from the International Tables of X-ray Crystallography, except for those of the hydrogen atoms, for which the contracted atom values of Stewart, Davidson, and Simpson[16] were used. Refinement includes positional and anisotropic thermal parameters for all non-hydrogen atoms, an isotropic extinction parameter, and the scale factor. Hydrogen atom parameters were fixed at their neutron-diffraction-determined values.

Full data (12 990 independent reflections) refinement was performed only with data $\geq 3\sigma(F_o^2)$. Two high-order refinements were also per-

(3) (a) Dunitz, J. D.; Seiler, P. *J. Am. Chem. Soc.* **1983**, *105*, 7056. (b) Savariault, J. M.; Lehmann, M. S. *J. Am. Chem. Soc.* **1980**, *102*, 1298.
(4) Cremer, D.; Kraka, E. *Angew. Chem., Int. Ed. Engl.* **1984**, *23*, 627.
(5) (a) Martin, M.; Rees, B.; Mitschler, A. *Acta Crystallogr., Sect. B: Struct. Crystallogr. Cryst. Chem.* **1982**, *B38*, 6. (b) Bénard, M.; Coppens, P.; DeLucia, M. L.; Stevens, E. D. *Inorg. Chem.* **1980**, *19*, 1924.
(6) Bénard, M. In *Electron Distributions and the Chemical Bond* edited by Coppens, P., Hall, M. B., Eds.; Plenum: New York, 1982; p 221.
(7) Trogler, W. C. *J. Chem. Educ.* **1980**, *57*, 424. This relation between the d–d overlap and the density accumulation at the center of the M–M bond has been confirmed by obtaining the first unambiguous electron buildup between two metal atoms for the shortest metal–metal bond observed in a stable system: the "supershort" Cr$\frac{4}{}$Cr bond.[8]
(8) Mitschler, A.; Rees, B.; Wiest, R.; Bénard, M. *J. Am. Chem. Soc.* **1982**, *104*, 7501.
(9) Wang, Y.; Coppens, P. *Inorg. Chem.* **1976**, *15*, 1122.
(10) Bénard, M. *J. Am. Chem. Soc.* **1978**, *100*, 7740.
(11) Baert, F.; Guelzim, H.; Coppens, P. *Acta Crystallogr., Sect. B: Struct. Sci.* **1984**, *B40*, 590.
(12) Coppens, P. *Acta Crystallogr., Sect. B: Struct. Crystallogr. Cryst. Chem.* **1974**, *B30*, 255.
(13) Cotton, F. A.; Jamerson, J. D.; Stults, B. K. *J. Am. Chem. Soc.* **1975**, *97*, 1774.
(14) Blessing, R. H.; Coppens, P.; Becker, P. *J. Appl. Crystallogr.* **1974**, *7*, 488.
(15) (a) Gregson, D.; Howard, J. A. K., private communication, 1982. (b) Gregson, D.; Howard, J. A. K. *Acta Crystallogr., Sect. C: Cryst. Struct.* **1983**, *C39*, 1024.
(16) Stewart, R. F.; Davidson, E. R.; Simpson, W. T. *J. Chem. Phys.* **1965**, *42*, 3175.

Table II. Atomic Positional Parameters[a]

	x	y	z	U_{eq}
Co(1)	24468 (3)	4922 (3)	23953 (2)	14 (1)
Co(2)	9699 (3)	24216 (3)	16335 (2)	13 (1)
C(1)	6308 (30)	−11179 (20)	27958 (20)	22 (1)
O(1)	−4869 (50)	−21327 (30)	30597 (30)	34 (2)
C(2)	29339 (30)	−3507 (30)	12603 (20)	25 (1)
O(2)	31993 (60)	−8866 (50)	5466 (20)	42 (2)
C(3)	40561 (40)	207 (30)	32157 (20)	27 (1)
O(3)	50441 (70)	−3288 (80)	37358 (40)	53 (4)
C(4)	−11904 (30)	11563 (30)	18088 (20)	19 (1)
O(4)	−25284 (30)	3565 (40)	19250 (30)	27 (1)
C(5)	12460 (30)	21076 (20)	3406 (20)	19 (1)
O(5)	14228 (40)	19108 (40)	−4735 (20)	28 (1)
C(6)	6198 (30)	44264 (30)	15181 (20)	23 (1)
O(6)	3796 (50)	56944 (40)	14221 (40)	39 (2)
C(10)	32974 (20)	29456 (20)	22750 (10)	15 (1)
C(11)	49780 (20)	41295 (20)	20229 (20)	17 (1)
C(12)	48146 (40)	58992 (30)	18777 (30)	31 (2)
C(13)	55765 (30)	35887 (40)	10812 (20)	25 (1)
C(14)	63112 (40)	41209 (50)	28850 (30)	22 (2)
C(20)	21623 (10)	25435 (10)	29680 (10)	14 (2)
C(21)	17842 (30)	29831 (30)	39864 (20)	19 (1)
C(22)	21631 (60)	48810 (40)	40731 (20)	31 (2)
C(23)	29016 (40)	23795 (40)	47783 (20)	27 (1)
C(24)	−850 (40)	21441 (50)	41779 (20)	29 (2)
H12(1)	396	596	123	39
H12(2)	434	633	252	69
H12(3)	605	677	176	35
H13(1)	466	354	46	29
H13(2)	578	237	115	44
H13(3)	676	447	89	29
H14(1)	594	456	357	40
H14(2)	645	290	302	32
H14(3)	753	497	272	18
H22(1)	140	535	351	72
H22(2)	182	519	480	65
H22(3)	347	553	399	45
H23(1)	262	104	478	56
H23(2)	425	290	466	28
H23(3)	270	276	551	43
H24(1)	−42	81	409	34
H24(2)	−91	264	368	27
H24(3)	−31	241	493	39

[a] The refinement is carried out until the numerator of the WR factor becomes invariant at least on the first decimal. In the present case, the changes affect only the sixth digit and can be considered to be zero (heavy atom values are $\times 10^5$, hydrogen values are $\times 10^3$, U_{eq} values are $\times 10^3$ Å^2, $U_{eq} = {}^1/_3\sum_i\sum_j U_{ij}\vec{a}_i^*\vec{a}_j^*\vec{a}_i\vec{a}_j$).

formed by varying all parameters as before, except the extinction parameter. The agreement factors are given in Table I. Final parameters from high-order refinement with $(\sin\theta)/\lambda = 0.85$ Å^{-1} are listed in Tables II and III. Ratios of the U_{ii}'s against the neutron values for all atoms are 1.15 (9) for r_{11}, 1.13 (7) for r_{22}, and 1.10 (9) for r_{33} where $r_{ii} = \sum U_{ii}(\mathrm{RXHO})/(\sum U_{ii}(\mathrm{neutron}))$ show a discrepancy of about 13% between the two experiments, so deformation density maps were calculated from the parameters of high-order refinements.

Peak intensities are strongly dependent on the cutoff in $(\sin\theta)/\lambda$ and on the threshold in $n\sigma(F_o^2)$. Their maximum value is obtained when all data with intensities $>\sigma(F_o^2)$ are included. However, the electron-deficient regions close to the Co atoms, which have a well-defined orientation with respect to the metal–metal axis ($\simeq 20°$), do not display this dependence, due to the higher average intensity of weak reflections.

The set of data has a resolution of 0.46 Å. To avoid in the least-squares refinement the bias coming from aspherical features, an alternative approach is to include parameters that describe the aspherical deformations of the molecular density. Static and dynamic electron density distributions have been obtained for model multipole expansions of real spherical harmonic functions according to the procedure proposed by Hansen and Coppens.[17] Details are reported in Table VI.

In order to determine the valence state of the Co atoms in the complex, different models were used in the multipole refinements. In model I, the 4s shell has been assumed empty (scattering table Co^{2+} Ar core, and $\langle j_0\rangle_{3d}$).[36] The first monopole is used to define the $3d^7$ shell. In model II, the $4s^2$ electrons have been included in the core and the scattering factors of Co are described as core^{20} + $3d^7$ (scattering table Co Ca core, and $\langle j_0\rangle_{3d}$).[36] In model III, the valence shell of cobalt is defined by two monopoles. Monopole 1 is defined as the 4s orbital of a free Co and the second monopole is attributed to the 3d shell.

An expansion coefficient κ is included to describe the first monopole of each atom (Table VII) in all models.

All the multipole models show improvement in the agreement factors compared to the case of conventional refinement. Each model shows that the cobalt atoms are positively charged. The static maps derived from models I and II tend however to yield density peaks that are very sharp and close to the cobalt nucleus. Model III is the only one to provide realistic values for the height and the location of peaks (see discussion below).

Electron Density Maps. The experimental X–X electron density distribution is displayed in plots of the deformation density $\Delta\rho$, defined as the difference between the total observed density and the density calculated from a superposition of spherical neutral Hartree–Fock atoms:

$$\Delta\rho = \rho(\mathrm{obsd})/k - \rho(\mathrm{spherical\ atoms}) = (1/V)\sum(F_o/k - F_c)e^{-i2\pi\mathbf{S}\cdot\mathbf{r}}$$

where k is the X-ray scale factor. Positional and thermal parameters used in calculating ρ(spherical atoms) were taken from high-order refinement. The deformation maps reported here were calculated with the use of the X-ray data to a resolution of $(\sin\theta)/\lambda = 0.90$ Å^{-1}, corrected for extinction and anomalous dispersion. Reflections with $I < 2\sigma(I)$ were eliminated. The scale factor was obtained by one cycle of refinement on k with all other parameters fixed at their high-order values.

Molecular Orbital Calculations. The theoretical density maps were obtained from ab initio LCAO–MO–SCF + CI calculations on $Co_2(CO)_6C_2H_2$, carried out with the ASTERIX system of programs, vectorized for the CRAY-1.[19] The Gaussian basis set used for Co was taken from the (13,7,5) set of Hyla-Kryspin et al.[20] and incremented with one p function of exponent 0.15 and one diffuse d function of exponent 0.08. It was contracted to [5,3,3], that is, minimal, for internal and 4p shells, double ζ for 4s shells and triple ζ for 3d shells. Basis sets (9,5) and (4) were used for first-row atoms and hydrogen, respectively,[21] and contracted to split valence, that is, [3,2] and [2].

The interatomic distances were taken from the most recent X-ray experimental determination.[22] The experimental structure of $Co_2(CO)_6C_2H_2$ is characterized by an asymmetrical disposition of the carbonyls but has been idealized into a perfect C_{2v} system here. The SCF calculation carried out on the closed-shell ground state yielded an energy of −3509.3680 au.

The configuration interaction (CI) expansion involved all single and double excitations arising from an active set of 34 MO's (19 taken from the occupied set and 15 from the virtual set). These MO's were selected according to the weight of their metal 3d population, so as to include in the active space most of the electrons of the 3d shells. More specifically, the active set of MO's included the frontier orbitals describing: (i) the metal–metal interaction (occupied bonding and virtual antibonding combinations); (ii) the σ donation from the carbonyl and acetylene ligands to the metal (with unoccupied counterparts); (iii) the π back-donation from the cobalt to CO and C_2H_2 (with unoccupied counterparts).

The population of the active space therefore contains an important part of the carbon lone pairs of carbonyls and of the π and π^* combinations of acetylene. However, this rather crude CI expansion, limited to single and double excitations within the valence shell, is not expected either to provide a high percentage of the total correlation energy or to describe quantitatively the electron reorganization associated with correlation. We just intend to check that, contrary to the case of binuclear systems with multiple metal–metal bonds,[8] the picture given by the SCF wave function is not deeply altered by correlation effects.

Discussion

Molecular Dimensions and Thermal Parameters. The molecule $Co_2(CO)_6C_2R_2$ with $R = C(CH_3)_3$ is shown in Figure 1. The essential characteristics of the molecular geometry observed in the crystal are reported in Table IV. The Co–Co bond length

(17) Hansen, N. K.; Coppens, P. *Acta Crystallogr., Sect. A: Cryst. Phys., Diffr., Theor. Gen. Crystallogr.* **1978**, *A34*, 909. See also: Baert, F.; Coppens, P.; Stevens, E. D.; Devos, L. *Acta Crystallogr., Sect. A: Cryst. Phys., Diffr., Theor. Gen. Crystallogr.* **1982**, *A38*, 143.
(18) Rees, B. *Acta Crystallogr., Sect. A: Cryst. Phys., Diffr., Theor. Gen. Crystallogr.* **1976**, *A32*, 483.
(19) Bénard, M.; Daniel, C.; Dedieu, A.; Demuynck, J.; Rohmer, M.-M.; Strich, A.; Veillard, A.; Wiest, R., to be submitted for publication.
(20) Hyla-Kryspin, I.; Demuynck, J.; Strich, A.; Bénard, M. *J. Chem. Phys.* **1981**, *75*, 3954.
(21) Huzinaga, S. *J. Chem. Phys.* **1965**, *42*, 1293.
(22) Baert, F., unpublished results.

Table III. Temperature Factors of Non-Hydrogen Atoms ($\times 10^4$)[a]

	U_{11}	U_{22}	U_{33}	U_{23}	U_{13}	U_{12}
Co(1)	144 (1)	107 (1)	130 (1)	5 (1)	11 (1)	45 (1)
Co(2)	124 (1)	122 (1)	121 (1)	−5 (1)	−4 (1)	42 (1)
C(1)	220 (7)	135 (5)	220 (7)	12 (5)	58 (6)	21 (5)
O(1)	342 (12)	199 (7)	353 (12)	16 (7)	147 (11)	−40 (8)
C(2)	267 (8)	184 (6)	163 (6)	−11 (5)	32 (5)	104 (6)
O(2)	463 (17)	314 (11)	238 (8)	−56 (7)	96 (9)	176 (11)
C(3)	237 (8)	240 (8)	205 (7)	23 (6)	−37 (6)	135 (7)
O(3)	403 (18)	511 (22)	334 (13)	74 (13)	−60 (12)	295 (18)
C(4)	144 (5)	190 (6)	202 (6)	−17 (5)	11 (5)	38 (5)
O(4)	147 (5)	279 (8)	343 (10)	−20 (7)	47 (6)	16 (5)
C(5)	188 (6)	178 (5)	142 (5)	−4 (4)	−1 (4)	60 (5)
O(5)	316 (9)	303 (9)	136 (5)	−26 (5)	5 (5)	108 (7)
C(6)	226 (7)	154 (6)	237 (8)	−10 (5)	−22 (6)	100 (5)
O(6)	363 (13)	197 (7)	444 (16)	10 (8)	4 (11)	154 (8)
C(10)	135 (5)	123 (4)	142 (4)	6 (3)	8 (4)	33 (3)
C(11)	142 (5)	150 (5)	193 (6)	6 (4)	18 (4)	22 (4)
C(12)	261 (10)	146 (6)	368 (14)	35 (7)	88 (9)	31 (6)
C(13)	182 (7)	242 (8)	223 (8)	1 (6)	63 (6)	28 (6)
C(14)	170 (7)	297 (11)	250 (9)	−1 (8)	−43 (7)	−2 (7)
C(20)	139 (1)	139 (1)	123 (1)	−10 (1)	1 (1)	41 (7)
C(21)	191 (6)	193 (6)	138 (5)	−27 (4)	9 (4)	70 (5)
C(22)	411 (16)	199 (8)	227 (8)	−57 (6)	34 (9)	107 (9)
C(23)	243 (9)	327 (11)	142 (6)	−18 (6)	−12 (5)	108 (8)
C(24)	210 (8)	364 (12)	172 (7)	−29 (7)	51 (6)	91 (8)

[a] $T = \exp[2\pi^2(U_{11}a_1^{*2}h^2 + U_{22}a_2^{*2}k^2 + U_{33}a_3^{*2}l^2 + U_{12}a_1^*a_2^*hk + U_{13}a_1^*a_3^*hl + U_{23}a_2^*a_3^*kl)]$.

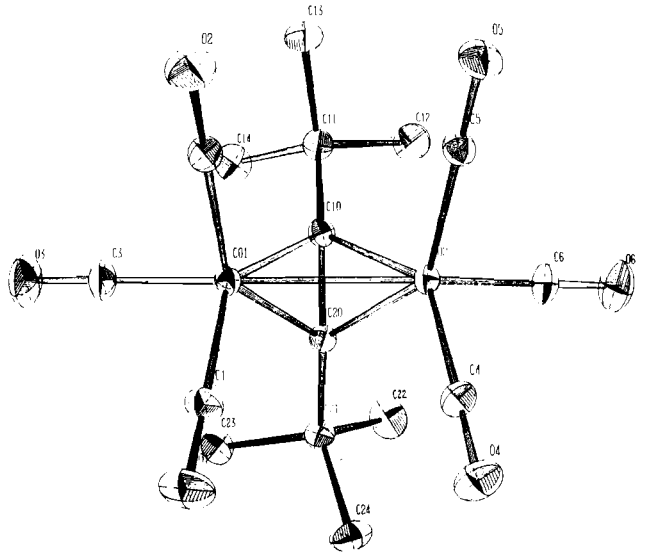

Figure 1. ORTEP representation of the $Co_2(CO)_6(C\text{-}t\text{-}Bu)_2$ complex.

is 2.462 Å and seems independent of the temperature and of the substituent on the acetylene derivative.[11] The two CO ligands trans to the acetylenic group have the averaged Co–C bond length 1.824 (2) Å, significantly longer than those of the Co–C ligands in cis positions (1.793 (2) Å). However, the C–O bond lengths (cis 1.139 (5) Å and trans 1.139 (4) Å) are not observed to be different.

These remarks have also been made[23] in connection with a study of the compound $Co_2(CO)_8$. It is tempting to correlate the differences in metal–CO distances with metal–ligand d → π back-bonding. However, results of that electron density study do not indicate significant differences between the cis and trans carbonyl groups. A rigid-body thermal-motion analysis[24] on the heavy atoms of the molecule has shown that the contributions of the internal modes of the C–O ligands and of the acetylenic derivative are negligible, the rms value of $U_{ij}^{obsd} - U_{ij}^{calcd}$ (rigid body) is of the order of $\sigma(U_{ij})$ (0.0030 Å^2 for the former compared to 0.0032 Å^2 for the latter).

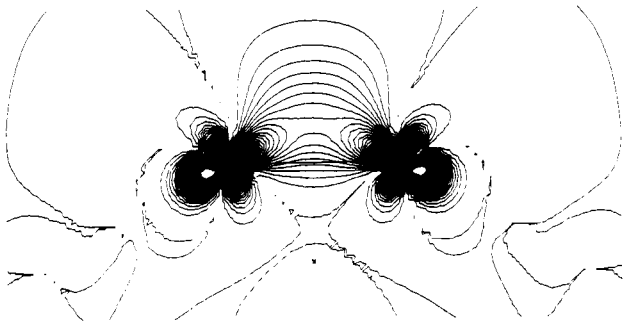

Figure 2. Total electron density generated by the HOMO of the LCAO–MO–SCF calculation carried out on $Co_2(CO)_6C_2H_2$. This section contains the two Co atoms and is perpendicular to the acetylene C–C bond (plane 1).

The U_{ij} values for the H atoms calculated from the TLS tensors previously determined are systematically lower than those independently determined from the least-squares refinement on neutron data. These differences emphasize the importance of the internal modes of vibration of the hydrogen atoms that cause problems in an X–X density study.

The translations are almost isotropic with an average amplitude of 0.18 Å. The off-diagonal elements of the libration tensor **L** referred to orthogonal axes defined on the unit cell are almost zero (see Table V). It can be assumed that the molecule librates around those axes. The moments of inertia have about the same values along the principal axes, and there is no preferential libration around one of these axes.

MO Calculations. Several quantum-chemical calculations have been performed on $Co_2(CO)_6C_2H_2$.[25,26] The first investigation was carried out by Thorn and Hoffmann by means of extended Hückel type (EHT) calculations.[25] This work rationalizes the origin of the "bent metal–metal bond" initially found by Teo et al. in $Fe_2(CO)_6X_2$ type complexes.[27] As shown by Thorn and Hoffmann, the bending of the M–M bond depends on the angle θ between the C_3 axis of the $M(CO)_3$ fragment and the metal–

(23) Holladay, A.; Leung, P.; Coppens, P. *Acta Crystallogr., Sect. A: Found. Crystallogr.* **1983**, *A39*, 377.
(24) Schomaker, V.; Trueblood, K. N. *Acta Crystallogr., Sect. B: Struct. Crystallogr. Cryst. Chem.* **1968**, *B24*, 63.
(25) Thorn, D. L.; Hoffmann, R. *Inorg. Chem.* **1978**, *17*, 126. Hoffmann, D. M.; Hoffmann, R.; Fisel, C. R. *J. Am. Chem. Soc.* **1982**, *104*, 3858.
(26) Van Dam, H.; Stufkens, D. J.; Oskam, A.; Doran, M.; Hillier, I. H. *J. Electron Spectrosc. Relat. Phenom.* **1980**, *21*, 47.
(27) Teo, B. K.; Hall, M. B.; Fenske, R. F.; Dahl, L. F. *Inorg. Chem.* **1975**, *14*, 3103.

Table IV. Bond Lengths (Å) and Bond Angles (deg)

Co(1)–Co(2)	2.462 (1)	C(1)–O(1)	1.138 (4)	C(20)—C(21)	1.516 (3)	C(14)–H(142)	1.072 (33)
Co(1)–C(1)	1.819 (2)	C(2)–O(2)	1.139 (4)	C(21)–C(22)	1.539 (4)	C(14)–H(143)	1.092 (34)
Co(1)–C(2)	1.828 (3)	C(3)–O(3)	1.137 (7)	C(21)–C(23)	1.536 (4)	C(22)–H(221)	1.091 (35)
Co(1)–C(3)	1.796 (3)	C(4)–O(4)	1.140 (4)	C(21)–C(24)	1.546 (4)	C(22)–H(222)	1.102 (30)
Co(1)–C(10)	1.984 (2)	C(5)–O(5)	1.146 (4)	C(12)–H(121)	1.097 (30)	C(22)–H(223)	1.078 (32)
Co(1)–C(20)	1.988 (1)	C(6)–O(6)	1.141 (4)	C(12)–H(122)	1.096 (32)	C(23)–H(231)	1.077 (24)
Co(2)–C(4)	1.830 (3)	C(10)–C(11)	1.519 (2)	C(12)–H(123)	1.097 (31)	C(23)–H(232)	1.098 (34)
Co(2)–C(5)	1.819 (3)	C(10)–C(20)	1.349 (2)	C(13)–H(131)	1.083 (30)	C(23)–H(233)	1.087 (40)
Co(2)–C(6)	1.791 (2)	C(11)–C(12)	1.538 (3)	C(13)–H(132)	1.082 (26)	C(24)–H(241)	1.079 (17)
Co(2)–C(10)	1.985 (2)	C(11)–C(13)	1.528 (4)	C(13)–H(133)	1.092 (33)	C(24)–H(242)	1.089 (29)
Co(2)–C(20)	1.983 (1)	C(11)–C(14)	1.546 (4)	C(14)–H(141)	1.106 (29)	C(24)–H(243)	1.095 (28)

Co(2)–Co(1)–C(1)	99.0 (1)	Co(1)–C(3)–O(3)	177.8 (4)	H(141)–C(14)–H(143)	107.6 (23)
Co(2)–Co(1)–C(2)	98.3 (1)	Co(2)–C(4)–O(4)	179.2 (3)	H(142)–C(14)–H(143)	109.0 (24)
Co(2)–Co(1)–C(3)	152.5 (1)	Co(2)–C(5)–O(5)	179.9 (2)	Co(1)–C(20)–Co(2)	76.6 (1)
Co(2)–Co(1)–C(10)	51.7 (1)	Co(2)–C(6)–O(6)	178.4 (3)	Co(1)–C(20)–C(10)	70.0 (1)
Co(2)–Co(1)–C(20)	51.6 (1)	Co(1)–C(10)–Co(2)	76.7 (1)	Co(1)–C(20)–C(21)	133.3 (1)
C(1)–Co(1)–C(2)	103.8 (1)	Co(1)–C(10)–C(11)	133.5 (1)	Co(2)–C(20)–C(10)	70.2 (1)
C(1)–Co(1)–C(3)	98.6 (1)	Co(1)–C(10)–C(20)	70.3 (1)	Co(2)–C(20)–C(21)	133.9 (1)
C(1)–Co(1)–C(10)	140.5 (1)	Co(2)–C(10)–C(11)	133.4 (1)	C(10)–C(20)–C(21)	144.1 (1)
C(1)–Co(1)–C(20)	102.8 (1)	Co(2)–C(10)–C(20)	70.0 (1)	C(20)–C(21)–C(22)	109.6 (2)
C(2)–Co(1)–C(3)	97.9 (1)	C(11)–C(10)–C(20)	144.3 (1)	C(20)–C(21)–C(23)	109.6 (2)
C(2)–Co(1)–C(10)	106.0 (1)	C(10)–C(11)–C(12)	110.0 (2)	C(20)–C(21)–C(24)	110.9 (2)
C(2)–Co(1)–C(20)	142.5 (1)	C(10)–C(11)–C(13)	111.2 (2)	C(22)–C(21)–C(23)	108.9 (2)
C(3)–Co(1)–C(10)	102.3 (1)	C(10)–C(11)–C(14)	108.6 (2)	C(22)–C(21)–C(24)	109.4 (2)
C(3)–Co(1)–C(20)	103.7 (1)	C(12)–C(11)–C(13)	109.1 (2)	C(23)–C(21)–C(24)	108.4 (2)
C(10)–Co(1)–C(20)	39.7 (1)	C(12)–C(11)–C(14)	109.5 (2)	C(21)–C(22)–H(221)	110.5 (18)
Co(1)–Co(2)–C(4)	97.6 (1)	C(13)–C(11)–C(14)	108.3 (2)	C(21)–C(22)–H(222)	109.5 (18)
Co(1)–Co(2)–C(5)	98.9 (1)	C(11)–C(12)–H(121)	111.1 (15)	C(21)–C(22)–H(223)	112.4 (16)
Co(1)–Co(2)–C(6)	152.0 (1)	C(11)–C(12)–H(122)	112.1 (17)	H(221)–C(22)–H(222)	106.7 (26)
Co(1)–Co(2)–C(10)	51.6 (1)	C(11)–C(12)–H(123)	109.8 (18)	H(221)–C(22)–H(223)	108.3 (24)
Co(1)–Co(2)–C(20)	51.8 (1)	H(121)–C(12)–H(122)	108.1 (23)	H(222)–C(22)–H(223)	109.2 (24)
C(4)–Co(2)–C(5)	104.2 (1)	H(121)–C(12)–H(123)	108.0 (23)	C(21)–C(23)–H(231)	111.6 (15)
C(4)–Co(2)–C(6)	99.3 (1)	H(122)–C(12)–H(123)	107.6 (24)	C(21)–C(23)–H(232)	111.1 (17)
C(4)–Co(2)–C(10)	141.2 (1)	C(11)–C(13)–H(131)	110.9 (17)	C(21)–C(23)–H(233)	110.2 (19)
C(4)–Co(2)–C(20)	104.4 (1)	C(11)–C(13)–H(132)	112.4 (15)	H(231)–C(23)–H(232)	107.8 (23)
C(5)–Co(2)–C(6)	98.4 (1)	C(11)–C(13)–H(133)	110.5 (17)	H(231)–C(23)–H(233)	107.8 (24)
C(5)–Co(2)–C(10)	103.7 (1)	H(131)–C(13)–H(132)	107.6 (23)	H(232)–C(23)–H(233)	108.1 (25)
C(5)–Co(2)–C(20)	141.3 (1)	H(131)–C(13)–H(133)	107.4 (24)	C(21)–C(24)–H(241)	111.9 (14)
C(6)–Co(2)–C(10)	102.7 (1)	H(132)–C(13)–H(133)	107.9 (23)	C(21)–C(24)–H(242)	110.2 (14)
C(6)–Co(2)–C(20)	102.1 (1)	C(11)–C(14)–H(141)	110.2 (17)	C(21)–C(24)–H(243)	109.7 (14)
C(10)–Co(2)–C(20)	39.8 (1)	C(11)–C(14)–H(142)	111.7 (17)	H(241)–C(24)–H(242)	109.5 (20)
Co(1)–C(1)–O(1)	178.8 (3)	C(11)–C(14)–H(143)	110.1 (17)	H(241)–C(24)–H(243)	107.9 (20)
Co(1)–C(2)–O(2)	178.4 (3)	H(141)–C(14)–H(142)	108.2 (24)	H(242)–C(24)–H(243)	107.6 (20)

Table V. Analysis of Rigid-Body Vibration Parameters for all Heavy Atoms of the Complex[a]

	principal axes									
	Å	deg	T, 10^{-4} Å^2			L, 10^{-4} rad^2			direction cos of L	
referred to orthogonal axes	0.1146	2.67	123 (9)	12 (7)	1 (7)	18 (1)	1 (1)	2 (1)	0.4262	0.0481	−0.9034
	0.1095	2.36		104 (9)	4 (7)		15 (1)	0 (1)	0.8900	0.1566	0.4282
	0.0976	2.18			121 (8)			21 (1)	0.1620	−0.9865	0.0238
	inertial moments		T, 10^{-4} Å^2			L, 10^{-4} rad^2			direction cos of inertial moments		
referred to inertial moments	38.25		102	11	93	16	1	14	0.7295	0.2934	0.6052
	35.59			123	58		17	8	−0.6337	0.6308	−0.4244
	38.13				110			17	0.2566	0.7183	0.6723

[a] Rms: $U^o - U^c = 0.0030$ Å^2; esd: $U_{obsd} = 0.0032$ Å^2.

metal line.[25] Due to the orientation of the $M(CO)_3$ groups, case **1** ($\theta = 58°$) corresponds to a straight metal–metal bond. This

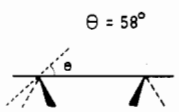

1

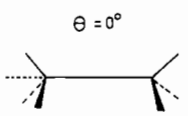

2

coupling is not favorable however due to a repulsive interaction with the acetylene donor orbital of proper symmetry.[25] A qualitatively similar situation occurs when the two $M(CO)_3$ fragments are replaced by the isolobal $M(C_5H_5)$ moieties. In fact, a bent metal–metal bond was also characterized for $Ni_2(Cp)_2C_2H_2$. The tilt angle θ is larger however between the C_5 axis of the Cp

Table VI. Type of Deformation with Local Symmetry Constraints and Number of Parameters/Atom

groups	atoms	symmetry site	no. of subsidiary params refined/atom
1	Co(1), Co(2)	m	15
2	C(10), C(20)	m	14
3	C(1), C(2), C(3),[a] C(4), C(5), C(6)	m	14
4	C(11), C(21)	m	14
5	C(12), C(13), C(14),[a] C(22), C(23), C(24)[a]	mm	9
6	O(1), O(2), O(3),[a] O(4), O(5), O(6)[a]	m	14
7	H atoms	mm[b]	1

[a] The deformation parameters of only the first atom of the group is refined. The values are listed for the other atoms of the group. [b] Only the dipole along the bond has been refined.

Table VII. Configuration of Co atoms and Multipole Refinement Results for Different Models[a]

	model I	model II	model III
κ	1.076 (2)	1.143 (1)	1.0
κ'	1.411 (42)	1.610 (39)	1.197 (17)
P_0	7.255 (23)	8.002 (24)	2
P_0'	0	0	6.296 (21)
P_{10} (z)	0.002 (19)	0.003 (27)	0.001 (15)
P_{11-} (y)	0.031 (19)	0.030 (28)	0.028 (16)
P_{20} $(2z^2 - x^2 - y^2)$	−0.236 (9)	−0.317 (9)	−0.250 (9)
P_{21-} (zy)	−0.029 (8)	−0.047 (8)	−0.025 (9)
P_{22-} $((x^2 - y^2)/2)$	0.030 (8)	0.080 (9)	0.013 (9)
P_{30} $(2z^3 - 3z(x^2 + y^2))$	0.028 (14)	0.031 (17)	0.027 (13)
P_{31-} $(y(4z^2 - (x^2 + y^2))$	−0.008 (13)	0.001 (16)	−0.009 (12)
P_{32+} $(3(x^2 - y^2))$	0.022 (14)	0.024 (16)	0.020 (12)
P_{33-} $(y^3 - 3yx^2)$	0.019 (13)	0.028 (16)	0.013 (12)
P_{40} $(8z^4 - 24z^2(x^2 + y^2) + 3(x^2 + y^2)^2)$	−0.033 (27)	−0.039 (36)	−0.025 (22)
P_{41-} $(y(4z^3 - 3z(x^2 + y^2)))$	0.131 (18)	0.167 (24)	0.110 (15)
P_{42+} $((x^2 - y^2)(6z^2 - (x^2 + y^2)))$	0.017 (26)	0.017 (34)	0.011 (21)
P_{43-} $(z(y^3 - 3yx^2))$	0.056 (25)	0.066 (34)	0.043 (21)
P_{44+} $(x^4 - 6x^2y^2 + y^4)$	0.053 (25)	0.071 (33)	0.042 (20)

[a] x and y are interchanged with respect to the Cartesian axes defined in Figure 3 and used in Table VIII.

ring and the Ni–Ni line (37°) than between the symmetry axis of $Co(CO)_3$ and the Co–Co line (26°), probably to relieve in this latter case the important carbonyl–carbonyl steric repulsion.[25] As a consequence, the bending of the metal–metal bond in the dicobalt system, visualized in Figure 2 from the electron density generated by the HOMO, is more pronounced than for the dinickel system. The difference of about 10° in the orientation of the bent metal–metal bond leads to most of the difference between the electron density maps computed for the two systems.

An important difference from the previous ab initio calculation of Van Dam et al. on $Co_2(CO)_6C_2H_2$[26] concerns the net atomic charges of cobalt and acetylene. These authors obtain a strong polarization of the system with large positive charges (+1.25 e) on the metal atoms and a corresponding negative charge (−0.62 e) on the acetylene carbons. An average charge of −0.26 e is reported for CO ligands. This polarization of the system is attributed by Van Dam et al. to the back-bonding charge transfers that populate the π_g^* antibonding MO's of the ligand.[26] Contrary to those results obtained with a relatively poor basis set, the present calculation displays moderate net charges on all atoms: +0.26 e for Co; −0.22 for acetylenic carbons. The CO ligands are close to neutrality. The present results do not mean that the electron transfers between metal and acetylene remain weak. The Mulliken population analysis shows that π back-donation accounts for an electron transfer of 0.88 e. This transfer is exactly balanced by the σ donation from the acetylene π-bonding orbitals to the cobalt, since the $(p_x + p_z)$ population of C_{ac} is 2.006 e. These results are in excellent agreement with a recent experimental study of the σ and π charge transfers in substituted μ-alkyne $Co_2(CO)_6$ systems.[28] That study, based on the measurement of the C_{ac}–C_{ac} stretching vibration frequency for a large variety of $Co_2(CO)_6$ RC≡CR complexes, shows that the σ and π transfers are almost balanced with some excess either for σ donation or for π back-donation, according to the nature of the ligand. For the class of alkyl or phenyl substituents the back-donation transfers account for 0.82–0.94 e.[28]

Density maps computed with respect to a superposition of molecular fragments demonstrate the decrease of the acetylene π-electron density and the corresponding population of the π^* orbitals (Figure 7).

The configuration interaction expansion (10400 configurations) yields an energy lowering of 0.292 au (0.360 including Davidson's correction for quadruple excitations). This energy change appears important, but it is directly related to the high number (38) of correlated electrons. In fact, this expansion shows that the SCF ground-state configuration is the only one of significant weight (77%). One other configuration, resulting from a single excitation, has a weight of 2%. Each of the remaining configurations contributes less than 1%. Concerning the molecular orbital populations, the main consequence of the CI expansion is a depopulation of the HOMO (from 2 to 1.897 e) mainly to the benefit of metal–metal antibonding MO's. Another weakly occupied MO with significant population (0.048 e) corresponds to the destabilized combination resulting from a repulsive interaction between the bent metal–metal bond and carbonyl π^* orbitals.[29]

Therefore, the main effect of CI is an electron transfer between orbital combinations located in the same region of space (mainly d_{z^2} and d_{xz} bonding and antibonding combinations). These transfers correspond to some weakening of the bent metal–metal bond—a very limited weakening however if compared to the effect of CI on the multiple metal–metal bond.[8] But since this limited electron reorganization does not correspond to charge transfers either between different atoms or at least between different metal d atomic orbitals, it is not expected to drastically modify the deformation density maps obtained at the SCF level.

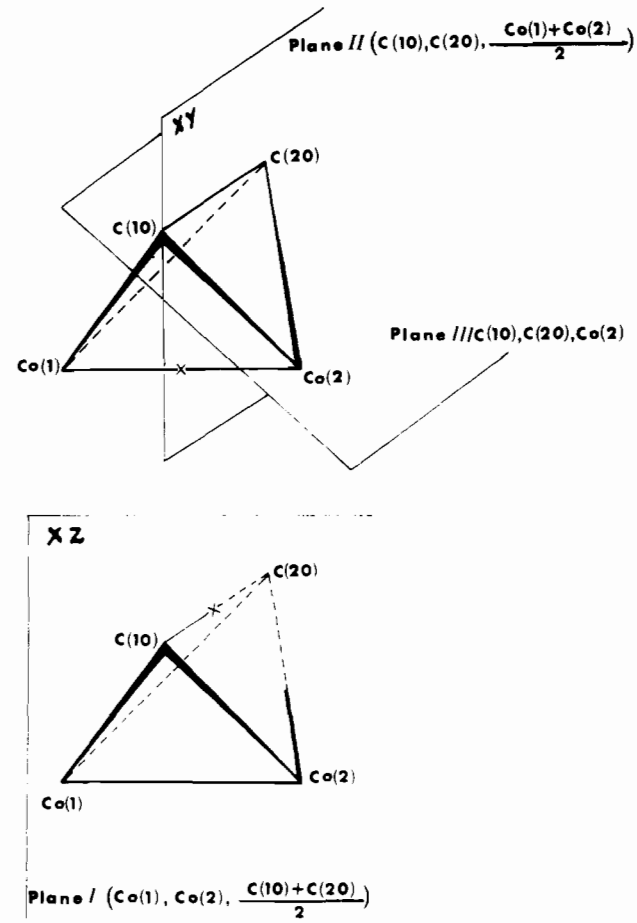

Figure 3. Representation of the sections of the deformation density distribution that are discussed in the present work. The z axis is collinear to the Co–Co direction, and the y axis is collinear to the acetylenic C–C bond.

Deformation Density Maps. For each section of chemical interest through the system five deformation density maps will be displayed, compared, and discussed in this section: (a) the map resulting from the X–X diffraction experiment carried out on $Co_2(CO)_6(C\text{-}t\text{-}Bu)_2$; (b) the static map obtained from multipole expansion (model III); (c) the dynamic map derived from the multipole model for planes 2 and 3; (d) the deformation density map computed from the CI wave function of $Co_2(CO)_6C_2H_2$ the

(28) Meyer, A.; Bigorgne, M. *Organometallics* **1984**, *3*, 1112.

(29) Due to back-bonding interactions, the four carbonyl ligands bent away from C_2H_2 contribute about 38% to the HOMO (see also ref 26).

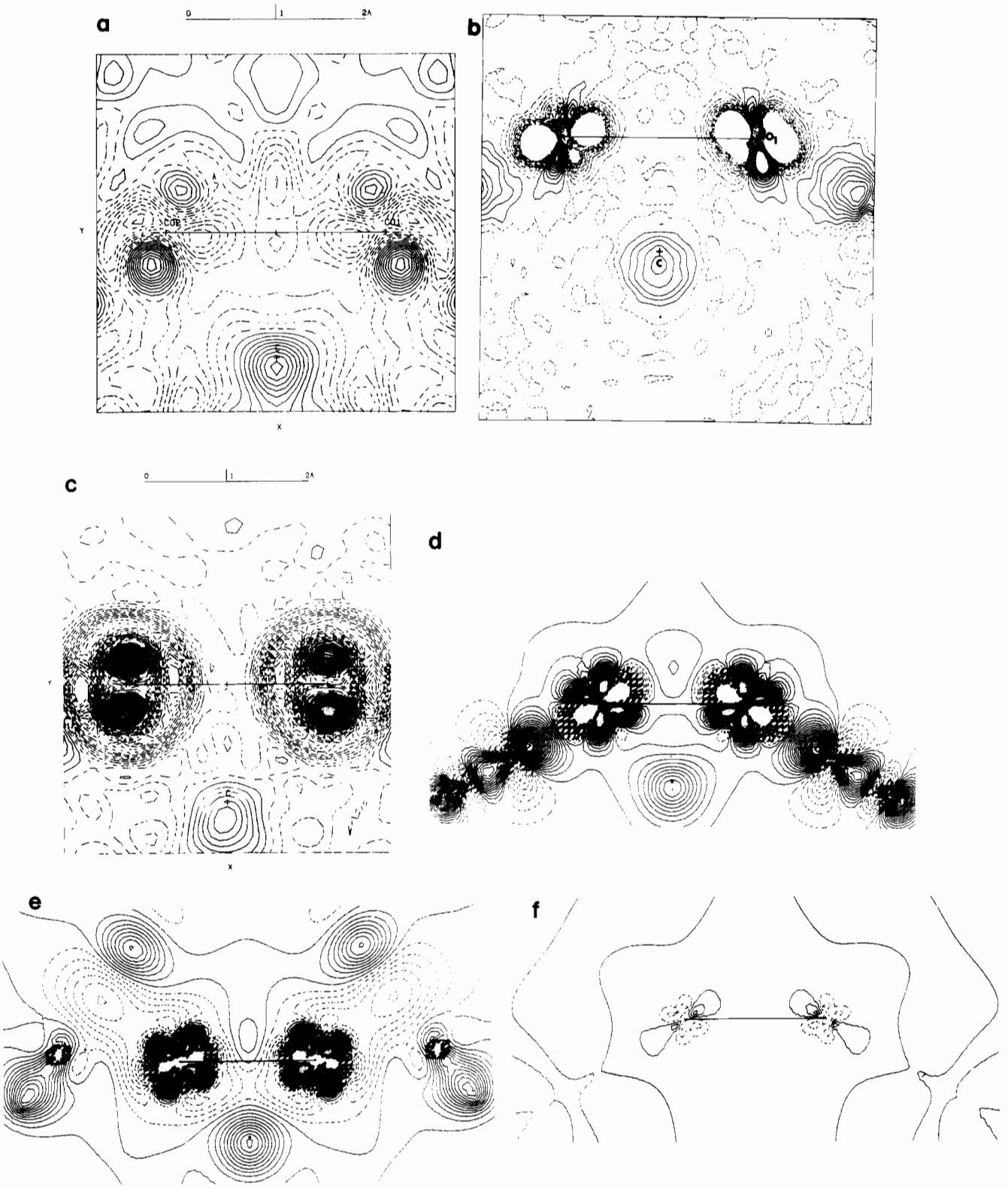

Figure 4. Electron deformation density maps in the plane containing the two metal atoms perpendicular to the acetylenic C–C bond (plane 1): (a) experimental (X–X) map for $Co_2(CO)_6(C\text{-}t\text{-}Bu)_2$ (contour spacing 0.05 e Å^{-3}, solid lines for positive contours, dashed lines for zero contour, dotted lines for negative contours); (b) "static" map from multipole refinement, model III (monopole 1 for $3d^7$, monopole 2 for $4s^2$; contour spacing 0.10 e Å^{-3}, solid lines for zero and positive contours, dashed lines for negative contours); (c) dynamic map from multipole refinement, model III (contours as in (a)); (d) theoretical map from the ab initio CI wave function for $Co_2(CO)_6C_2H_2$ (contour spacing 0.05 e Å^{-3}, solid lines for zero and positive contours, negative contours dashed); (e) theoretical map from an ab initio SCF wave function for $Ni_2(Cp)_2C_2H_2$[9] (contour spacing as in (d)); (f) correlation density (difference between the density distributions computed at the CI and at the SCF levels) for $Co_2(CO)_6C_2H_2$ (contour spacing as in (d)).

difference map for one of the sections (plane 1), between the CI and the SCF wave function, being displayed; (e) the deformation density map computed in a previous work[10] for $Ni_2(Cp)_2C_2H_2$ (SCF level). The static and dynamic model maps have not been averaged to account for the symmetry of the system.

Three sections have been selected (Figure 3): (i) Plane 1 contains the two metal atoms and the midpoint of the acetylene C–C bond. (ii) Plane 2 contains the C_{ac}–C_{ac} axis and the midpoint of the metal–metal axis. (iii) Plane 3 contains the C_{ac}–C_{ac} axis and one metal atom.

Plane 1. The most prominent features in the observed (X–X) map (Figure 4a) are the two density peaks of 0.2 and 0.45 e Å^{-3} in the neighborhood of the Co atoms (0.35 and 0.50 Å, respectively, from the metal) and the peak corresponding to the section of the C_{ac}–C_{ac} bond. At variance from the X–X maps reported by Wang and Coppens for $Ni_2(Cp)_2C_2H_2$,[9] no accumulation of density is observed between the two cobalt atoms.

The static maps computed from the multipole coefficients of models I and II display four very sharp lobes (7–8 e Å^{-3}) around the cobalt atoms. The shape of the lobes and their orientation are in agreement with the theoretical maps (Figure 4d). The strongest lobes that are the farthest from the center of the atom are also present on the experimental deformation map, whereas the nearest ones, due to the lack of resolution, are completely absent.

The set of data has a resolution of 0.46 Å. Refinement through a mathematical model is expected to improve the resolution, but the results will become strongly model-dependent. In fact, in models I and II we observe an important contraction of the density toward the Co atoms. The value of κ for these two models converges to 1.41 and 1.61, respectively, which corresponds to 0.41 and 0.35 Å for the point of maximum d-electron density generated by the radial function for the cobalt atoms. The range of R is probably too short for the model to account for electron density located relatively far from the metal atoms.

The refinement with model III, where the $3d^7$ shell is introduced in monopole 2, yields a value of κ converged to 1.19. The static map obtained from this model (Figure 4b) shows that the peak heights in the vicinity of the cobalt (1–1.4 e Å^{-3}) become much more realistic. Two peaks only are obtained around each cobalt (Figure 4b) and correspond to the peaks of the experimental map (Figure 4a). The two other peaks obtained from models I and II and from the theoretical maps do not show up with model III, and they are replaced by an extension of the main electron-deficient region with lower density gradient and distinct minima (Figure 4b). These main electron-deficient regions located around the Co atoms represent the other remarkable feature of the static map. By joining the density minima through the metal nucleus, one can obtain at each cobalt atom an axis of minimum density that defines the direction of the metal–metal bent bond, in remarkable agreement with the computed map (Figure 4d).

Reconvolution of the thermal motion using model III yields the dynamic map displayed in Figure 4c, which is directly comparable to that of Figure 4a. As for plane 3, no dramatic distortion has occurred during the deconvolution and reconvolution process, except for a significant increase of the density gradient.

In the computed map (Figure 4d) each cobalt atom is surrounded by four peaks of similar height (about 2 e Å^{-3}). The metal–metal axis remains, however, in a depopulated environment. A diffuse accumulation region with a low peak (0.1 e Å^{-3}) is obtained at the center of the metal–metal bent bond. This density peak is not present in the X–X and in the model maps.

The computed map for $Ni_2(Cp)_2C_2H_2$ (Figure 4e) is qualitatively very similar to the one obtained for $Co_2(CO)_6C_2H_2$, at least in the vicinity of the metal atoms. The angle made by the "axes of minimum density" with the metal–metal line is smaller for the dinickel than for the dicobalt complex, in accordance with the slightly different orientation of the metal–metal bent bond discussed above.

It may appear surprising that the metal–metal bond is characterized by a depopulation region with a double minimum running along the bent bond line except in the central region. In fact, the metal–metal covalent bond is built from the overlap of two d type orbitals populated each with about one electron.[30] Since the average d-orbital population of cobalt in the promolecule is 1.4 e (1.6 e for nickel), the direction of the metal–metal bond must obviously be characterized by an electron deficiency. At the center of the bond however the d–d overlap, which is known to be very weak at distances of about 2.5 Å,[7] generates the diffuse accumulation obtained in the computed maps. Similar cases have been recently observed in the field of organic chemistry,[3,4] and a rationalization of these "bonds without electron buildup" has been recently given by Spackman and Maslen.[31] These authors argue that the condition $\Delta\rho > 0$ between the nuclei is neither necessary nor sufficient for binding and that a decrease of ρ *outside the nuclei*, along the internuclear axis, can also generate an attractive electrostatic force.[31]

The difference map relating the CI and the SCF computed density distributions (Figure 4f) shows that the electron reorganization due to CI is almost negligible. In this difference map, the region located between the metal atoms remains slightly negative, indicating that CI somewhat reduces the region of accumulation associated with the bent Co–Co bond (the contour at +0.1 e Å^{-3} at the center of the bond is more extended in the map derived from the SCF wave function, not reproduced here).

Plane 2. The observed map (Figure 5a), the model static map (Figure 5b), and the computed map (Figure 5c) display the "acetylene bent bond" where the density peak is shifted away from the Co–Co line rather than concentrated on the C_{ac}–C_{ac} axis. A similar feature had also been obtained by Wang and Coppens for $Ni_2(Cp_2)C_2H_2$ even though the density was split into two separate peaks located in the vicinity of the acetylene carbons.[9] It may appear surprising that the density peak is shifted *away* from the Co–Co line even though the carbon σ orbitals are tilted *toward* the Co–Co line due to the deformation of the acetylene system. This can be understood from the well-known deformation density pattern in a single ethane-like (**3**) and in a standard acetylenic

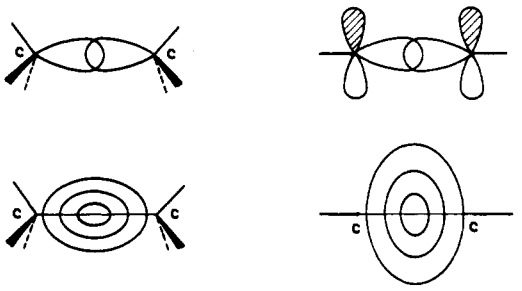

3 **4**

(**4**) C–C bond. The occurrence of the π bond in **4** extends the accumulation region above and below the C–C line, but a unique peak is found on the C–C axis. If the acetylenic system is distorted as in **5**, the σ overlap will occur below the C–C line, but the overlap

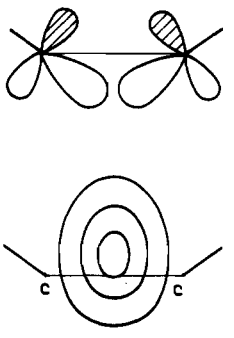

5

of π orbitals will concentrate *above* this line. For a tilt angle of 37°, the unique peak resulting from the σ and π overlap will be shifted in the same direction as the C–R bonds.

(30) According to the Mulliken population analysis, the population of the cobalt d_{xz} orbitals (with lobes at 45° from the metal–metal axis) is 1.18 e. A d-type orbital collinear to the bent bond (about 30° from the Co–Co axis) would be still less populated.

(31) Spackman, M. A.; Maslen, E. N. *Acta Crystallogr., Sect. A: Found. Crystallogr.* **1985**, *A41*, 347.

(32) The SCF population of the metal d shell in the complex is 7.88 e for CO and 8.86 e for Ni. These numbers must be used with caution, however, since they were not obtained from similar basis sets.[9]

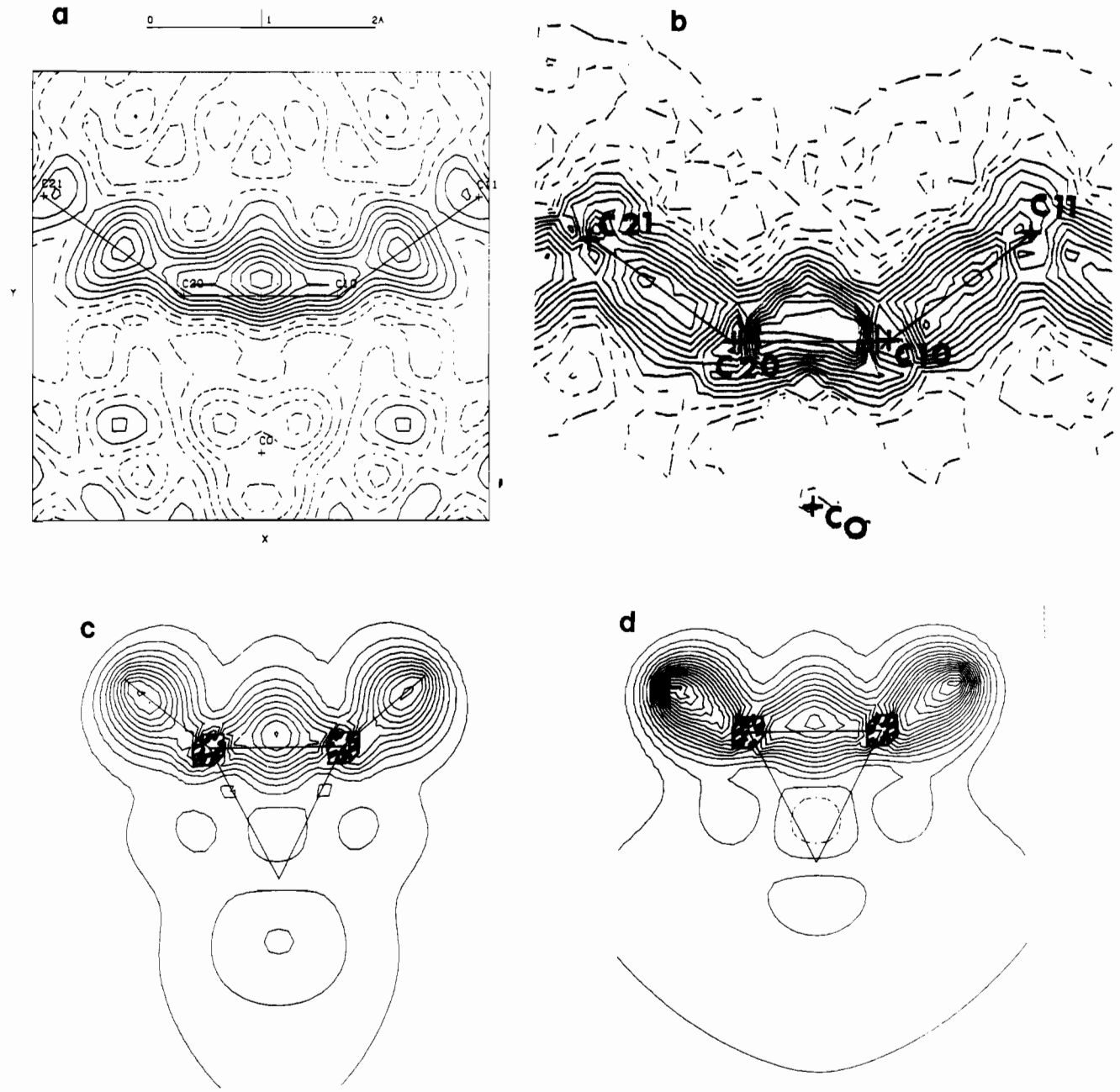

Figure 5. Electron deformation density in the plane containing the two acetylene carbons perpendicular to the metal–metal line (plane 2): (a) experimental (X–X) map for $Co_2(CO)_6(C\text{-}t\text{-}Bu)_2$ (contours as in Figure 4a); (b) static map from multipole refinement, model III (contours as in Figure 4b); (c) theoretical map (CI level) for $Co_2(CO)_6C_2H_2$ (contours as in Figure 4d); (d) theoretical map (SCF level) for $Ni_2(Cp)_2C_2H_2$[9] (contours as in Figure 4d).

Plane 3. Plane 3 contains one cobalt and the two acetylenic carbon atoms. The observed map (Figure 6a) displays again the accumulation associated with the C–C bond with a central peak shifted away from the Co atom. The accumulation region extends however toward the cobalt atom (Figure 6a), accounting for the σ donation from the acetylenic π system to the cobalt. Each carbon atom is surrounded by two negative zones located at the position of the p_π orbitals. These negative regions can be interpreted as resulting from the electron shift toward the center of the acetylenic system to form the π bond. Similar density minima are obtained in the computed map (Figure 6d).

In the vicinity of the Co atom, the observed map (Figure 6a) shows two small peaks symmetric with respect to the metal. The electron-deficient surrounding is structured in the static map into four negative lobes, in excellent agreement with the computed map (Figure 6d).

At variance with the two other planes, the plane 3 map computed for the dinickel system (Figure 6e) appears qualitatively different from that of $Co_2(CO)_6C_2H_2$. Four negative lobes are still present around the metal, but the main features are four strong peaks orientated parallel and perpendicular to the C_{ac}–C_{ac} line. These changes are explained by the high population of the t_{2g}-like orbitals in the dinickel complex and more specifically of the d_{xz} orbital (1.863 e)[6] compared to that of $Co_2(CO)_6C_2H_2$ (1.18 e). Even though Co(0) and Ni(I) are isoelectronic, the d shell of nickel remains much more electron rich in the complex (total population of the metal d shell in the complex: 7.88 e for Co; 8.86 e for Ni). Furthermore, following the different orientation of the metal–metal bond, which is more bent in the cobalt than in the nickel system, the bonding MO in the nickel complex is mainly d_{z^2} with some d_{xz} character, while in the cobalt complex, it is an equal mixture of the d_{z^2} and d_{xz} orbitals. The consequence is a relatively low population for only the d_{z^2} orbital in the nickel system (1.48 e) but for both d_{z^2} and d_{xz} in the cobalt complex (Table VIII).

d-Orbital Populations. Holladay, Leung, and Coppens[23] have presented in a recent paper generalized formulas relating multipole population parameters to d-orbital occupancies of transition-metal atoms. We have applied these expressions to the three multipole

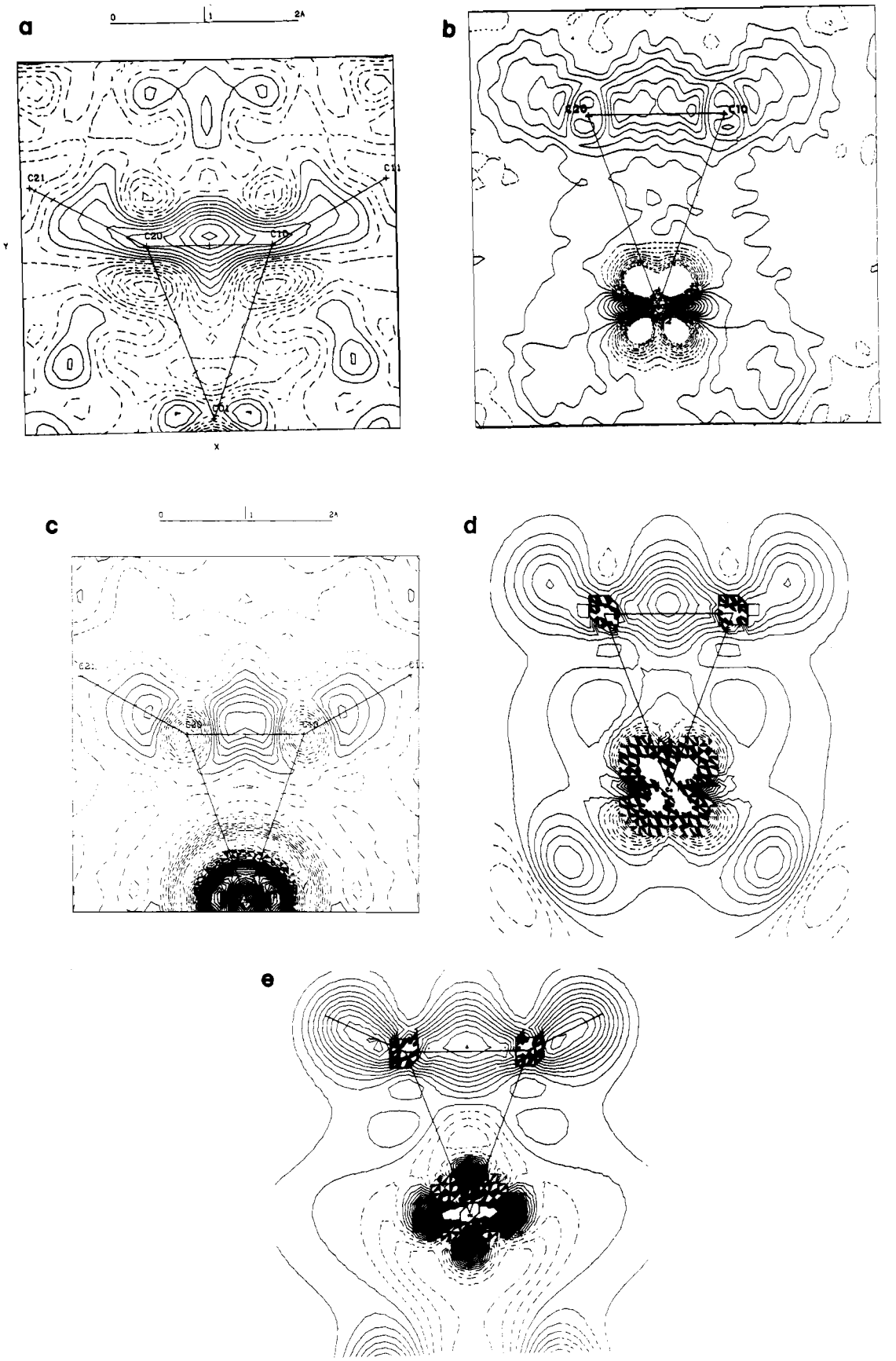

Figure 6. Electron deformation density maps in the plane containing the two acetylene carbons and one metal atom (plane 3): (a) experimental (X–X) map for $Co_2(CO)_6(C\text{-}t\text{-}Bu)_2$ (contours as in Figure 4a); (b) static map from multipole refinement, model III (contours as in Figure 4b); (c) dynamic map from multipole refinement, model III (contours as in Figure 4a); (d) theoretical map (CI level) for $Co_2(CO)_6C_2H_2$ (contours as in Figure 4d); (e) theoretical map (SCF level) for $Ni_2(Cp)_2C_2H_2$[9] (contours as in Figure 4d).

refinement models defined above for $Co_2(CO)_6(C\text{-}t\text{-}Bu)_2$. The results are reported in Table VIII.

Contrary to the results reported for $Cr(CO)_6$ and other carbonyl complexes,[23] we noticed a strong dependence of the total d-shell population upon the choice of the model (Table VIII). In that sense, none of the models, assuming the 4s shell to be occupied with either 2 e (models II and III) or 0 e (model I), compare quantitatively with the populations obtained from quantum chemical calculations. The contribution of the 4s/4p shell in the CI wave function is 0.92 e.

The asphericity deduced appears, however, consistent for all three models, and some trends can be deduced from a comparison with the Mulliken population analysis. Three classes of d orbitals can be characterized:

(i) The d_{z^2} and the d_{xz} orbitals (x perpendicular to the Co–Co (z) and to the C_{ac}–C_{ac} (y) directions) are both involved in the bent metal–metal bond, which is responsible for their electron-deficient character. They account for about 33% of the d-shell population.

(ii) The $d_{x^2-y^2}$ does not take part in any strong σ or π interaction with the ligands and can be considered as a lone-pair-type orbital. Its population consistently represents about 24% of the total d-shell population.

(iii) The d_{xy} and d_{yz} orbitals are slightly more populated than in the spherical model (about 43%).

The comparison between model and theoretical orbital populations appears however quantitatively inaccurate when the population of individual orbitals in analyzed (Table VIII). This is probably related to the dubious character of space partitioning especially regarding the contribution of the diffuse 4s and 4p shells of metal atoms.[33]

Fragment Deformation Densities. The promolecule considered as a superposition of neutral atoms provides a useful reference for comparison between the observed and the computed density distributions. The information of chemical interest is more easily obtained and interpreted, however, if the deformation density distribution is interpreted in terms of a reorganization of the electron cloud resulting from the chemical interaction between molecular *fragments*. Such a description of the molecule is easy to obtain in quantum-chemical calculations: it only requires one to define the promolecule as a superposition of molecular fragments in their ground state, the wave function for each fragment being computed with the same basis set and at the same level of accuracy as the whole system.[34,35]

A fragment deformation density calculation has been carried out for $Co_2(CO)_6C_2H_2$ by partitioning the complex into three sections:

$$2Co(CO)_3 + C_2H_2$$

The wave function for the $Co(CO)_3$ fragments has been computed at the CI level, including in the active space, as for the whole system, all MO's with significant 3d metal weight.

The fragment deformation denisities are displayed in Figure 7a–c for planes 1–3, respectively.

As in the case of $Mn_2(CO)_{10}$ and $RCCo_3(CO)_9$,[34] the fragment deformation density enhances the accumulation region associated with the metal–metal bond (Figure 7a). The peak height is now close to 0.2 e Å^{-3} (cf. 0.1 e Å^{-3} in the standard map obtained with regard to a superposition of atoms). One can conclude with Hall[34] that the rearrangement due to the formation of the cobalt–carbonyl bonds results in a net loss of electron density between metal atoms. It is possible to go one step further and to associate the loss of density in the Co–Co bond region with the decrease of the population of shell 4 induced by the field of CO ligands.[6] In other words, the positive net charge of the metal when subject to the ligand field tends to uniformly contract the sphere of outer valence electrons. This isotropic contraction with respect to the isolated metal atom contributes to erase the peak associated with the d–d overlap. It is interesting to notice in that connection that the accumulation region associated with the nickel–nickel bond (net charge of nickel +0.82) is lower and less extended (+0.05 e Å^{-3}) than that generated by the cobalt–cobalt bond (0.10 e Å^{-3} with a net charge of +0.26 e on the cobalt; see Figure 4d,e).

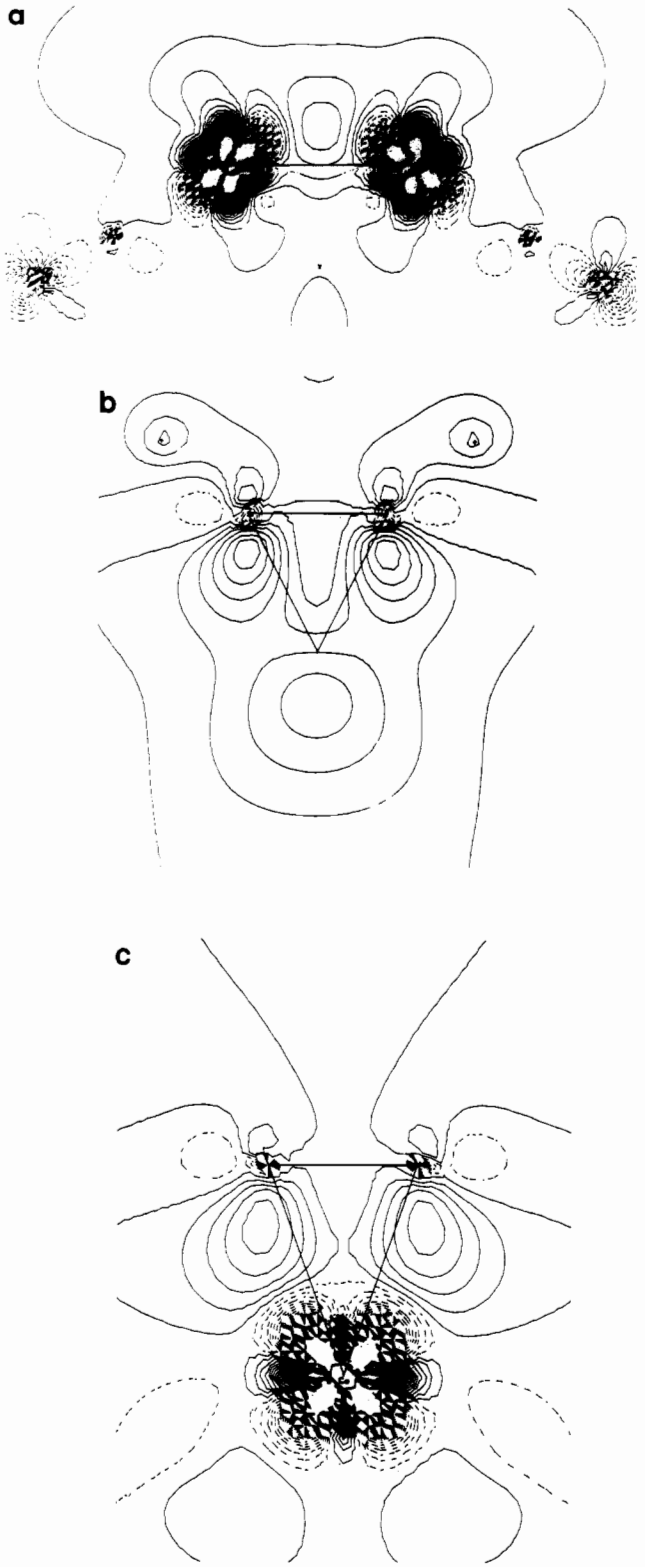

Figure 7. Theoretical fragment deformation density maps (CI level) for $Co_2(CO)_6C_2H_2$ with regard to the superposition of $2Co(CO)_3 + C_2H_2$ (contours as in Figure 4d): (a) plane 1 (containing Co–Co and the midpoint of C_{ac}–C_{ac}); (b) plane 2 (containing C_{ac}–C_{ac} and the midpoint of Co–Co); (c) plane 3 (containing C_{ac}–C_{ac} and one cobalt atom).

The main feature observed in planes 2 and 3 from the fragment deformation densities (Figure 7b,c) is the substantial population of carbon π^* orbitals. The region of the acetylene π bond remains,

(33) Coppens, P. *Coord. Chem. Rev.* **1985**, *C5*, 285.
(34) See for instance: Hall, M. B. Reference 6, p 205.
(35) Bénard, M.; Dedieu, A.; Nakamura, S.; *Nouv. J. Chim.* **1984**, *8*, 149.
(36) *International Tables for X-ray Crystallography*; Kynoch: Birmingham, England, 1974; Vol. IV.

Table VIII. d-Orbital Populations of the Co atoms in $Co_2(CO)_6C_2R_2$ for the different Models and from the CI Wave Function (Mulliken Population Analysis)

	model I[a]		model II[a]		model III[a]		theor[b]	
	popln	% of total	popln	% of total	popln	% of total	popln	% of total
d_{z^2}	1.16 (4)	16.0	1.22 (5)	15.3	0.96 (3)	15.3	1.49	19.0
d_{xy}	1.60 (4)	22.1	1.80 (5)	22.6	1.44 (3)	22.9	1.53	19.6
d_{xz}	1.30 (4)	18.0	1.37 (5)	17.2	1.12 (3)	17.8	1.18	15.1
d_{yz}	1.41 (4)	19.5	1.57 (5)	19.7	1.18 (3)	18.7	1.77	22.6
$d_{x^2-y^2}$	1.77 (4)	24.4	2.00 (5)	25.1	1.58 (3)	25.1	1.85	23.7
total	7.25		7.96		6.28		7.82	

[a] See Table VII. [b] Mulliken population analysis carried out on the CI wave function.

however, electron deficient due to the donation from acetylene to the metal. Finally, plane 2 (Figure 7b) displays a continuous accumulation region from one acetylenic carbon to the center of the Co–Co bent bond and then back to the second acetylenic carbon. Even though the bent metal–metal bond and the back-donation toward acetylene are separate interactions that involve MO's belonging to different irreducible representations, they both contribute to an important electron delocalization throughout the region defined by cobalt atoms and acetylenic carbons. As for carbonyl-bridged binuclear systems,[35] the term "multicentered linkage" can be used to characterize the chemical interaction between the dimetal system and the acetylenic fragment.

Conclusion

This study reports electron deformation density maps for $Co_2(CO)_6(C\text{-}t\text{-}Bu)_2$ observed from low-temperature X-ray diffraction experiments. Static deformation densities obtained from multipole refinement are compared to a theoretical distribution issued from ab initio MO–SCF + CI calculations carried out on $Co_2(CO)_6C_2H_2$. These results are discussed in relation with experimental and theoretical density maps previously obtained for the isolobal system $Ni_2(Cp)_2C_2H_2$. The main conclusions are as follows:

(a) The experimental, static, and theoretical maps show that a region of electron deficiency is oriented along the axis of the bent metal–metal bond. At the center of this bond, the deformation density is close to zero, slightly negative in the experimental and model maps, but slightly positive in the computed one. A similar discrepancy between X-ray diffraction results and quantum-chemical calculations has already been reported for the metal–metal bonding region of $Cr_2(O_2CCH_3)_4$.[5b]

(b) In the plane containing the Co–Co line, perpendicular to C_{ac}–C_{ac}, the static maps derived from two of the above multipole models display four distinct density peaks around each cobalt, as in the computed map. The third multipole model however generates only two peaks. In the other planes considered an excellent agreement is obtained between the static and the computed maps.

(c) The CI expansion carried out for $Co_2(CO)_6C_2H_2$ indicates that the effect of correlation in the reorganization of electron density is negligible in this system.

(d) The calculated π back-donation from cobalt to acetylene amounts to 0.88 e, in excellent agreement with the experimental results of Meyer and Bigorgne,[28] based on the measurement of the C–C stretching frequency in a series of $Co_2(CO)_6$ RC≡CR complexes. This back-donation is balanced by a σ-donation charge transfer of similar amount.

(e) The theoretical deformation density distribution computed at the CI level for $Co_2(CO)_6C_2H_2$ is similar to the distribution previously computed for the isolobal system $Ni_2(C_5H_5)_2C_2H_2$ with minor differences due to the more electron-rich character of the nickel d shell and due to the slightly different orientation of the metal–metal bent bond.

(f) At variance from the computed distributions, the experimental (X–X) deformation density maps observed for $Co_2(CO)_6(C\text{-}t\text{-}Bu)_2$ and $[Ni(C_5H_5)]_2C_2H_2$[9] are strinkingly different. It seems that the density accumulation with a double maximum observed along the Ni–Ni axis of the latter compound is an artifact resulting from the crystalline acentric and disordered structure of this complex.[9]

Acknowledgment. The quantum-chemical calculations have been carried out on the CRAY-1 of the CCVR (Palaiseau) through a grant of computer time from the Conseil Scientifique du Centre de Calcul Vectoriel pour la Recherche. J.M.P. is grateful to the French Government for a grant.

Registry No. $Co_2(CO)_6C_2(t\text{-}Bu)_2$, 59687-97-7.